


# Hubbard $U$ parameters for transition metals from first principles

Rebekka Tesch 

*Institute of Energy and Climate Research, Theory and Computation of Energy Materials (IEK-13),  
Forschungszentrum Jülich GmbH, 52425 Jülich, Germany;  
Chair of Theory and Computation of Energy Materials, Faculty of Georesources and Materials Engineering,  
RWTH Aachen University, 52062 Aachen, Germany;  
and Jülich Aachen Research Alliance, JARA-CSD and JARA-ENERGY, 52425 Jülich, Germany*

Piotr M. Kowalski 

*Institute of Energy and Climate Research, Theory and Computation of Energy Materials (IEK-13),  
Forschungszentrum Jülich GmbH, 52425 Jülich, Germany  
and Jülich Aachen Research Alliance, JARA-CSD and JARA-ENERGY, 52425 Jülich, Germany*



(Received 20 July 2021; revised 6 May 2022; accepted 9 May 2022; published 31 May 2022)

Using the linear response-based constrained local density approximation (cLDA) approach we systematically computed the Hubbard  $U$  parameters for series of  $3d$ ,  $4d$ , and  $5d$  transition metals. We compare the results with estimations by the constrained random phase approximation (cRPA) method and discuss the performance of the self-consistent density functional theory +  $U$  (DFT +  $U$ ) method for prediction of lattice parameters, work functions,  $d$ -bandwidths and  $d$ -band centers. Interestingly, we found that blindly applied the standard, fully localized limit (FLL) version of the DFT +  $U$  approach heavily overestimates the positions of  $d$ -band centers with respect to the Fermi level, but much better agreement with experiment is obtained when applying a more realistic, Wannier-type representation of  $d$  orbitals for projection of  $d$  states occupancies. We present another, independent estimate of the Hubbard  $U$  parameter based on the comparison of Hartree-Fock and DFT eigenvalues, and positions of  $d$ -band centers. The so-derived estimates are surprisingly well consistent with the ones derived from the above-mentioned first principles approaches, and allow for validation of cRPA or cLDA results for the disputed cases, including Cu, Ag, and Au for which large  $U$  parameters are obtained from the cLDA method.

DOI: [10.1103/PhysRevB.105.195153](https://doi.org/10.1103/PhysRevB.105.195153)

## I. INTRODUCTION

Density functional theory is the most successful and widely used quantum chemical simulation approach [1–6]. Nevertheless, it has limitations in correctly describing highly localized, strongly correlated  $d$  or  $f$  electrons [7–11]. A computationally inexpensive and therefore very popular way to correct for these deficiencies is the density functional theory +  $U$  (DFT +  $U$ ) approach [12–14]. However, this method requires the knowledge of the Hubbard  $U$  parameter that describes the effective Coulomb on-site electron-electron interaction and, in some cases, also the knowledge of the Hund exchange interaction parameter  $J$  [8,15]. The selection of these parameters for a particular computational problem is usually made by semiempirical fitting of calculated properties to the relevant experimental data (e.g., lattice parameters, band gaps or reaction enthalpies), or simply by using a “reasonable” value [16–21]. On the other hand, there exist methods to compute these parameters from first principles, making the DFT +  $U$  method a fully parameter-free, first principles-based technique.

A variety of methods have been used to derive the Hubbard  $U$  parameter. It can be obtained from the difference

in total energy of electronic configurations with the number of  $d$  or  $f$  electrons increased and decreased by one (e.g.,  $2d^n \rightarrow d^{n-1} + d^{n+1}$ ) [22–26]. Another *ab initio* approach relies on molecular orbitals from unrestricted Hartree-Fock calculations and the relation of the  $U$  and  $J$  parameters to the Slater integrals [27,28]. The  $U$  parameter can also be calculated from the average on-site Coulomb matrix elements computed with the aid of the maximally localized Wannier functions basis set [25]. An accurate but computationally intensive method is based on the constrained random phase approximation (cRPA) [15,29–31]. It allows for accounting for or excluding different screening channels in the evaluation of the Hubbard  $U$  parameter, an important aspect broadly discussed in the context of Hubbard  $U$  parameters derivation by different methods [8,15,32]. This method has been applied to systematically derive the Hubbard  $U$  parameter for  $d$  metals [15]. An alternative to the cRPA method is the linear response approach, which is one of the realizations of more generalized constrained local density approximation (cLDA) [8,33], which is computationally inexpensive and thus feasible for computation of large systems that contain even hundreds of atoms [10]. In this framework, the Hubbard  $U$  parameter is obtained from the perturbation-induced variation of the occupation number of the  $d$  or  $f$  orbitals [8]. The cLDA method has been shown to perform well for transition metal

\*p.kowalski@fz-juelich.de

oxides [8,34] as well as  $4f$  and  $5f$  elements [9,10]. Although there exist systematic derivations of the Hubbard  $U$  and  $J$  parameters for elemental transition metals [15], application of the cLDA method has been limited to  $3d$  metals only [26,31]. The correct values of Hubbard  $U$  and  $J$  parameters are important as they may affect the position of the  $d$ -band, which is of utmost importance for the correct modeling of adsorption behavior and catalytic activity of metal surfaces [35], for which standard DFT often does not yield the desired accuracy [36–38]. Knowledge of the Hubbard  $U$  parameter is also required for advanced calculations of electronic structure of condensed matter, using, for instance, the dynamical mean field theory (DMFT) [15,33], a method that is considered as suitable for accurate computation of transition metals [39]. On the other hand, it has been speculated that the standard DFT approach is more appropriate for computation of metals than the DFT +  $U$  method [11,40]. Another variant of the DFT +  $U$  approach, “the around mean field approach” (AMF) has been also proposed for computation of metals [40–42], in which the DFT +  $U$  scheme forces the delocalized occupations of  $d$  electrons taking as a reference a mean value, as opposite to the fully occupied or unoccupied orbitals in the standard DFT +  $U$  approach, called “the fully localized limit” (FLL) [42,43]. A combination of AMF and FLL methods has been also proposed to improve the description of electronic structure of materials, including metals, by the DFT +  $U$  method [40].

Systematic investigation of the impact of the Hubbard  $U$  correction on the computed properties of transition metals has not been performed before. The DFT +  $U$  method has been occasionally used in studies of Fe, Co, and Ni [8,44,45], but in general, the standard DFT is most commonly used to describe pure transition metals (e.g., Hofmann *et al.* [46]). We note that the necessity of applying the DFT +  $U$  method for weakly correlated (early)  $d$  metals is debated [40], but the line between weakly and moderately correlated systems is not clearly defined. Instead, for weakly correlated metals, the mentioned AMF version of the DFT +  $U$  method [41] has been proposed, and shown to give good results [8]. On the other hand, Jain *et al.* [11] demonstrated empirically that the standard DFT computation of metals results in much better formation enthalpies of transition metal oxides, although the application of the DFT +  $U$  method has been shown to be essential for the considered oxide phases. Nevertheless, independently of its necessity or importance, when properly applied, the DFT +  $U$  method should give good results also for pure metal systems [47].

In this study, we performed systematic derivation of the effective Hubbard  $U$  parameters with the cLDA method for all  $3d$ ,  $4d$ , and  $5d$  transition metals. We aimed to compare the obtained results with the values predicted with the cRPA method and computed applying  $sp$  screening (Fig. 2 of Şaşıoğlu *et al.* [15]), to make it directly comparable with the results of cLDA method [8,32] and with an estimate we made based on Hartree-Fock calculations. We also intended to test the performance of the DFT +  $U$  method on a large set of available experimental data on  $d$  metals, including lattice parameters, magnetic moments, work functions,  $d$ -bandwidths, and  $d$ -band centers.

## II. METHODOLOGY

All calculations were performed with the Quantum ESPRESSO software package [48]. Ultrasoft and norm-conserving pseudopotentials were used to describe the core electrons with no differences in computed parameters. We applied plane-wave energy cutoffs of 50 and 150 Ry for ultrasoft and norm-conserving pseudopotentials, respectively. We used the PBEsol exchange correlation functional [49] with some comparative calculations performed with the PBE functional [50]. The PBEsol functional has been specifically used as it results in much better prediction of structural parameters [49] and thus allows for more meaningful comparison with the experimental lattice parameters. A Monkhorst-Pack [51]  $k$ -point mesh of  $8 \times 8 \times 8$  (or comparable for noncubic cells) was applied to assure converged results. All structures were optimized with convergence thresholds of  $10^{-5}$  Ry and  $10^{-4}$  Ry/ $a_0$  (where  $a_0$  is the Bohr radius) for energy and forces, respectively. Except for a few magnetic cases (Cr, Mn, Fe, Co, Ni), all metals were computed as spin unpolarized.

The Hubbard  $U$  parameter considered here is an effective Hubbard parameter  $U_{\text{eff}} = U - J$ , where  $J$  is the Hund exchange term [8]. For simplicity, from here on by the  $U$  parameter reported through this paper we mean the  $U_{\text{eff}}$ . This parameter is derived here by applying the linear response method of Cococcioni and de Gironcoli [8]. These calculations were performed on  $2 \times 2 \times 2$  supercells, which we found to give sufficient convergence in terms of system size. We note that there are differences between the applied procedure and that of the cRPA method regarding accounting for screening. While the cRPA method implicitly accounts for the  $sp$  screening, it excludes the  $d$  screening compound (the value computed in such a way is taken as the Hubbard  $U$  parameter) [15]. On the other hand, the linear response method does not require any *a priori* assumptions about the screening [8].

The Hubbard  $U$  parameters were calculated for all  $3d$ ,  $4d$ , and  $5d$  transition metals in their most common, low-temperature crystal structures, i.e., fcc for Ni, Cu, Rh, Pd, Ag, Ir, Pt and Au; bcc for V, Cr, Fe, Mn, Nb, Mo, Ta and W; and hcp for Sc, Ti, Co, Y, Zr, Tc, Ru, Lu, Hf, Re and Os. For those  $3d$  metals that show magnetic properties in their crystalline bulk phases, magnetic states were additionally considered; namely: ferromagnetic (FM) states for Mn, Fe, Co and Ni and an antiferromagnetic (AFM) state for Cr [15].

The standard DFT +  $U$  calculations discussed here were performed in the FLL scheme with the discussions of the aspects of the AMF approach [40,42]. As an alternative to the standard atomic orbitals set of  $d$  orbital projectors for the DFT +  $U$  calculations, we used maximally localized Wannier functions [52]. This was done with the aid of poor man’s wannierization scheme as implemented in the Quantum ESPRESSO package (pmw.x tool), excluding the  $4s$  states from the procedure. All calculations involving the Wannier-functions-based representation were performed as single points calculations using geometries from the standard atomic orbital-based DFT +  $U$  calculations. This is because forces are currently not implemented for such a computational setup in the standard release of the Quantum ESPRESSO package. The

wannierization scheme was not used in the calculation of Hubbard  $U$  parameters.

In order to calculate work functions, surfaces were represented by slabs of five atomic layers thickness. We applied a 30 Å thick vacuum layer between the periodically repeated slabs. The  $k$ -point mesh for surface calculations was  $8 \times 8 \times 1$ . To preserve the bulk environment at the bottom of the slab, the two bottom layers were fixed during geometry optimization.

### III. RESULTS AND DISCUSSION

#### A. Hubbard $U$ parameters from cLDA

Figure 1 shows the Hubbard  $U$  parameters derived here by the cLDA method, together with the theoretical and experimental reference data. 3d metals show the largest  $U$  values, and  $U$  decreases with increasing  $d$  element row number. This effect has been also observed for the  $U$  parameters calculated with the cRPA method [15] and reflects the higher degree of localization of 3d states. The calculated  $U$  parameters exhibit strong trends along the  $d$  element rows. The  $U$  values are smaller than 1 eV for early transition metals, and increase continuously with filling of the  $d$  shell. Such a trend is expected due to the increasing number of  $d$  electrons (and more pronounced correlation effects). The increase in nuclear charge and the resulting stronger localization of  $d$  orbitals also contributes to the rise in correlation effects. The same trend is visible in the series of  $U$  parameters computed by Şaşıoğlu *et al.* [15] with the cRPA method. The trend of increasing  $U$  with increasing  $d$  shell filling, seen in both computed data sets, is in line with the experimental data [53–56], the independent cLDA derivations [14,26,32,58] and calculations by other *ab initio* methods [14].

Our calculations show that the spin-polarization has a strong effect on the  $U$  parameter for the magnetic 3d elements. Except for the case of antiferromagnetic Cr, all magnetic states show significantly smaller  $U$  values than the nonmagnetic cases, by 0.7 to 2.2 eV. We note that we cannot explain this effect by change in the lattice parameters, which results in much smaller variation in the derived  $U$  parameter values ( $\sim 0.1$  eV). The cRPA study by Şaşıoğlu *et al.* [15] does not show so pronounced differences between the magnetic and nonmagnetic states.

The largest differences between the Hubbard  $U$  parameters obtained with the cLDA and cRPA methods are for Cu, Ag, and Au, i.e., the latest transition metals, with the cLDA method resulting in significantly larger values that are well out of the trends clearly formed by all other members of the series (Fig. 1). Such large, and usually not applied  $U$  parameters were also obtained in previous cLDA studies for these elements. For Cu Nakamura *et al.* [26] obtained 9.0 eV and Schnell *et al.* [25] report a very large value of 18.2 eV, although the later value may be overestimated because of computing a one atom unit cell. Cu, Ag, and Au have completely filled  $d$  shells and the cLDA approach is known to give unreasonable results for such cases [15,31]. This may happen because the polarization of  $d$  to non- $d$  orbitals is not correctly captured by the cLDA approach for atoms with completely filled  $d$  shell, since hopping between, for instance,

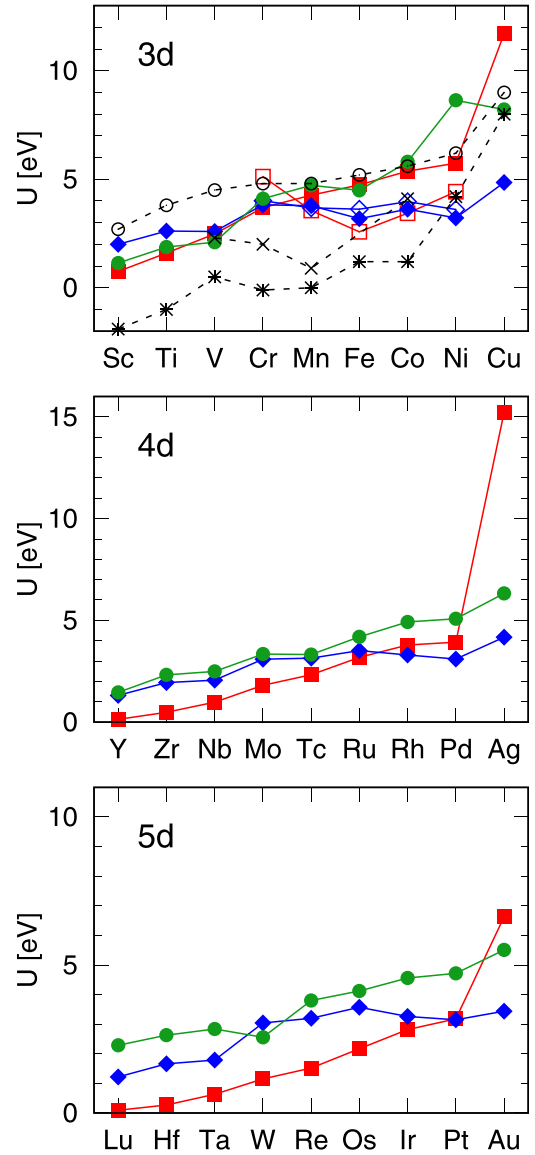


FIG. 1. The Hubbard  $U$  parameters for 3d, 4d, and 5d transition metals. The different symbols denote the results obtained with: the cLDA method (red filled and open squares for nonmagnetic and magnetic metals, respectively), the  $d$ -band center shifts between HF and DFT methods (green circles for nonmagnetic metals), the cRPA method by Şaşıoğlu *et al.* [15] (blue filled and open diamonds for nonmagnetic and magnetic metals, respectively), the cLDA method by Nakamura *et al.* [26] (open circles). The black symbols represent the experimental values (the measured correlation energy deduced from Auger and XPS spectroscopy) of de Boer *et al.* [53], Sawatzky and Post [54], Antonides *et al.* [55] (stars) and Kaurila *et al.* [56] (crosses, with uncertainty at the level of  $\pm 0.4$  eV). We note, however, that an exact correspondence between the measured and computed values is not expected and we provide these values only for qualitative comparison. All the reported data are also provided in the ESI, Table S2 [57].

3d and non-3d states is cut off due to the constrained (maximum) 3d electron number on the completely filled  $d$  site [31]. This may also lead to incorrect screening [15]. On the other hand, the experimental value of 8.0 eV [56] obtained for Cu

from Auger spectroscopy indicates larger  $U$  values for late transition metals, as compared to the other transition metals. These values will be validated later by comparison of the calculated electronic density of states (DOS) with the x-ray photoelectron spectroscopy (XPS) data.

In the next section we present another, independent, estimate of the Hubbard  $U$  parameters for transition metals that is based on Hartree-Fock calculations.

### B. Hubbard $U$ parameters using Hartree-Fock results as a reference

We propose here that an estimate of the Hubbard  $U$  parameter could be made using the Hartree-Fock (HF) method. HF is an exact method for the exchange part of the electronic interaction, but does not account for the correlations. However, comparing to DFT, HF results in reasonable estimates of eigenvalues. For instance, by applying Koopmans' theorem [59] HF reproduces the experimental ionization potentials of single atoms with relative errors of only  $\sim 1$  eV [60]. On the other hand, DFT heavily underestimates the eigenvalues, including the one of the highest occupied orbital, which should correspond to the ionization energy. The standard DFT +  $U$  method could be seen as a cure for such a deficiency [8]. In principle, it shifts the occupied electronic levels by  $-0.5 U$  [61]. So, we assumed that the Hubbard  $U$  parameter can be estimated as

$$U = 2(\epsilon_{\text{DFT}} - \epsilon_{\text{HF}}), \quad (1)$$

where  $\epsilon_{\text{DFT}}$  and  $\epsilon_{\text{HF}}$  are the DFT and HF eigenvalues, respectively. To our knowledge, such an approach has not been used before, although Schnell *et al.* [25] used similar reasoning to explain the difference between the eigenvalues computed for selected metals with Hartree and unscreened Hartree-Fock approximations.

We note that such a derivation based on the comparison of DFT and HF results seems contradictory, as the DFT +  $U$  method is expected to correct for electronic correlations effects, neglected completely by the HF method. However, it is well known that, for instance, the PBE0 exchange-correlation functional [62] corrects the DFT (PBE) prediction for strongly correlated elements (e.g., Refs. [10,63]), while having the same description of correlations as the PBE functional and differing only by the exchange part (by mixing HF with PBE exchange) [62,64]. It has been also realized that the DFT +  $U$  approach provides a better description of exchange than DFT, by reducing the self-interaction problem [39]. In our estimate, HF results serve only as a reference that gives more realistic estimate of orbitals energies.

In the first step we thus compared the HF eigenvalues of the highest occupied  $d$  orbitals with the ones derived by DFT and interpret differences as a shift by  $-0.5 U$ . In Table I we compare the so-derived  $U$  parameter to the estimates by cLDA and cRPA. For fcc metals, with the exception of Au, the HF estimate matches the  $U$  values derived from cRPA and/or cLDA surprisingly well. This may be related to the fact that fcc metals are always late transition metals. For bcc and hcp metals, HF values are slightly larger than cRPA values, and much larger than cLDA values. For Mo, the method results in a small negative value.

TABLE I. The Hubbard  $U$  parameter estimated from the differences between Hartree-Fock and DFT  $d$  orbitals eigenvalues, by considering the shift of the highest occupied level (high. occ.) and the shift of the  $d$ -band center (dbc). The last row represents the same estimate for the lowest occupied valence  $s$  states (4s, 5s, and 6s). The  $U$  values computed with the cLDA and cRPA methods are reported for comparison. All values are in eV.

	Ti	V	Cu	Mo	Rh	Ag	W	Pt	Au
Structure	hcp	bcc	fcc	bcc	fcc	fcc	bcc	fcc	fcc
cLDA	1.6	2.5	11.7	1.8	3.8	15.2	1.2	3.2	6.6
cRPA [15]	2.6	2.6	4.9	3.1	3.3	4.2	3.0	3.2	3.4
HF (high. occ.)	3.8	3.5	5.0	-0.1	3.7	3.5	4.6	2.6	1.1
HF (dbc)	1.9	2.1	8.2	3.3	4.9	6.3	2.6	4.7	5.5
HF ( $s$ states)	11.4	12.6	11.1	12.4	12.1	9.5	12.3	12.5	11.1

In the second step, we made the same estimate, but by comparing the differences in the positions of  $d$ -band centers obtained from the DFT and HF simulations. With such an approach we account for the cumulative relative shifts of all the  $d$  states. For most of the cases, the resulting  $U$  values provided in Table I and in Fig. 1 are larger than the estimate based solely on the highest occupied eigenvalues, but more consistent with the cLDA and cRPA results. In fact, the trends of increased  $U$  parameter values along the  $d$  elements series are well captured. Surprisingly, such a HF-based estimate matches well the results of the cRPA method for early 3d and 4d transition metals.

We were particularly interested in the estimate for Cu, Ag and Au, in order to understand the differences in results from the cLDA and the cRPA methods (see Fig. 1), and to check if with the HF-based derivation, we could validate large  $U$  values for these elements. We obtained  $U$  parameters of 5.0 and 8.2 eV for Cu and 3.5 and 6.3 eV for Ag with the HF estimates from the highest occupied level and the  $d$ -band center shifts, respectively, which are consistent with the values computed by the cRPA method, but far smaller than the cLDA values. This estimate thus independently shows that the cLDA method indeed overestimates the Hubbard  $U$  parameter values for transition metal elements with completely filled  $d$  shells. We also note that the HF estimate for Au of 1.1 eV, based on the highest occupied level only, is much smaller than the values obtained by cRPA or cLDA methods. However, the HF estimate of 5.5 eV based on the position of the  $d$ -band center falls between the cLDA and the cRPA values, which is similar to the case of Cu. Our exercise thus shows that the HF-based calculations are useful in estimation of the Hubbard  $U$  parameters.

We note, however, that the HF method does not provide a perfect description of the electronic states of  $d$  metals. When comparing the DOS computed for Cu (see Fig. 2) to the reference data, we notice that our DFT results match other DFT calculations well [25,65,66]. However, unscreened HF calculations by Schnell *et al.* [67] show the Cu 3d-band at 22 eV below the Fermi level and far distant from the Fermi level 4sp states [67]. Our HF DOS also shows the  $d$ -band at large distance ( $\sim 10$  eV) from the Fermi level. Schnell *et al.* [67] attribute the difference in HF and DFT DOS to the



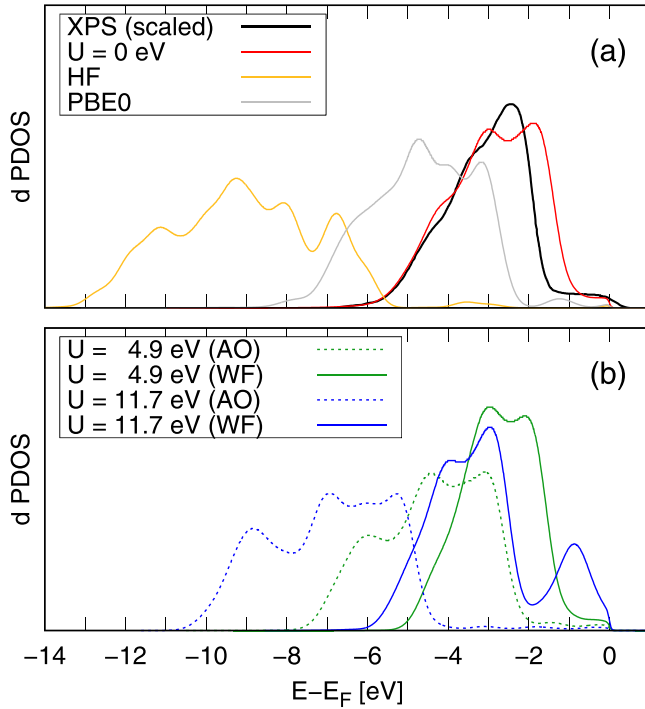


FIG. 2. The projected  $d$  orbitals density of states for fcc Cu metal: (a) computed with the standard DFT ( $U = 0$ ), hybrid functional (PBE0) and Hartree-Fock methods, as well as measured with XPS by Ref. [46], and (b) computed with DFT +  $U$  and different projections of the  $d$  states occupancy: atomic orbitals (AO), Wannier functions (WF). Gaussian smearing of 0.03 Ry has been used to match the experimental band broadening. The XPS data are scaled vertically to match the intensity of the computed  $d$ -band.

electronic self-interaction, which is correctly treated in HF, but not in DFT. On the other hand, experimental spectra [65,66,68] show that plain DFT calculations match the  $d$ -band position much better than the HF calculations of Schnell *et al.* [67]. We observe this also in our studies.

In order to validate the Hubbard  $U$  parameter values obtained with different methods, in the next section we test the performance of the DFT +  $U$  method for prediction of a set of physical parameters.

### C. Evaluation of $U$ parameters

It is well known that different derivation methods can result in some differences in the derived Hubbard  $U$  parameters [8,69]. The reason for that is, for instance, different projectors used for projection of occupancies of orbitals of interest (e.g.,  $d$  orbitals) [8,70]. As pointed out by Cococcioni and de Gironcoli [8], the best approach is to self-consistently apply the same method to derive the  $U$  parameter and to perform the follow-up calculations of targeted properties. We thus applied our derived  $U$  values for the calculation of lattice parameters,  $d$ -bandwidths and  $d$ -band centers for all  $d$  transition metals as well as work functions for the selected cases. The resulting values are compared to those estimated by standard DFT calculations and by DFT +  $U$  calculations with the  $U$  parameter values derived by the cRPA method [15], keeping in mind that

TABLE II. Relative errors in % of computed lattice parameters for selected metals obtained with different computational methods, taking the experimental values as a reference [71,72]. The full table is available in the ESI, Table S3 [57].

		DFT	DFT + $U$ (cLDA)	DFT + $U$ (cRPA)
Ti	hcp ( $a$ )	-1.29	-0.65	-0.19
	hcp ( $c$ )	-1.48	-0.71	-0.17
V	bcc	-2.18	-2.15	-2.15
Cu	fcc	-0.77	+0.61	-0.27
Zr	hcp ( $a$ )	-1.21	-1.16	-0.98
	hcp ( $c$ )	-0.21	-0.22	-0.24
Mo	bcc	-0.26	-0.70	-0.98
Rh	fcc	-0.39	-1.15	-1.06
Ag	fcc	-0.04	+1.31	+0.35
W	bcc	-0.33	-0.64	-1.09
Os	hcp ( $a$ )	-0.23	-0.76	-1.11
	hcp ( $c$ )	+0.23	-0.44	-0.83
Pt	fcc	+0.41	+0.02	+0.02
Au	fcc	+0.76	+1.22	+0.99

the cRPA values were derived using computational setup and software that are different from the ones applied here.

One important aspect of the DFT +  $U$  calculations is the double counting scheme applied in the calculations. The applicability of the standard DFT +  $U$  approach in the FLL scheme is broadly discussed in the literature [8,42] and often the AMF scheme is suggested as a correct approach for computation of metals [42]. The two schemes represent the extreme limits, with the FLL scheme forcing full localization of the considered electrons with the occupation of the relevant orbitals being “1” or “0”, and the AMF scheme forcing complete delocalization with the orbitals occupation resembling the average electronic density [40,42]. However, it was demonstrated that the real solution may be better represented by a hybrid between the two extremes [40], with the AMF and FLL approaches more appropriate for metals with small ( $U < 2$  eV) and large ( $U > 2$  eV) Hubbard  $U$  parameter, respectively. Because the AMF scheme for uniform occupations of  $d$  orbitals results is a solution equivalent to the standard DFT (because of the vanishing of equivalent Hubbard energy and potential terms [40]), here we just focus on the discussion of the result of application of the standard FLL-based DFT +  $U$  approach to the metals. This part is important because of the widespread usage of the FLL scheme. However, the discussion should be followed keeping in mind that the FLL method by design may not be fully appropriate for description of metallic systems.

Table II shows the signed relative errors of computed lattice parameters for selected  $d$  metals in different crystal structures (the full table is available in the ESI). We note that the reference experimental values were corrected for thermal expansion effects using the measured linear thermal expansion coefficients [72]. Because we applied the PBEsol exchange-correlation functional that by design gives good predictions for lattice parameters of solids, the standard DFT gives good results for most of the considered metals. The DFT +  $U$

TABLE III. The computed and measured magnetic moments per atom for magnetic 3d metals (using atomic orbital projectors). The cRPA  $U$  parameters are those of Şaşıoğlu *et al.* [15]. The  $U$  parameter values (in eV) used in the calculations are given in parentheses. All values are in  $\mu_B$ .

	Cr	Mn	Fe	Co	Ni
	AFM	FM	FM	FM	FM
	bcc	bcc	bcc	hcp	fcc
DFT	$\pm 0.50$	0.59	2.13	1.63	0.63
DFT + $U$ (cLDA)	$\pm 3.80$ (5.1)	3.89 (3.6)	2.56 (2.6)	1.63 (3.4)	0.62 (4.4)
DFT + $U$ (cRPA)	$\pm 3.60$ (4.0)	3.89 (3.7)	2.66 (3.6)	1.63 (4.0)	0.63 (3.6)
exp. spin magn. mom.	$\pm 0.59$ [76] <sup>a</sup>		2.13 [77]	1.53 [77]	0.57 [77]

<sup>a</sup>This is the total magnetic moment, which includes the orbital magnetic moment. The spin magnetic moment should be slightly smaller.

calculations with the  $U$  parameter derived by either the cLDA or the cRPA methods show very similar performance. Agreement with the experimental values is best for fcc and bcc, and slightly worse for hcp structures. We obtained larger errors for magnetic cases, which are related to wrongly reproduced magnetic moments for Cr and Mn, which we discuss later. Overall, most of the lattice parameters are predicted with the relative errors smaller than 2 %, which is in the usual accuracy range of DFT methods [73]. The lattice parameters of some metals (e.g., Fe, Pd, and Pt) are surprisingly well predicted by the DFT +  $U$  calculations.

Table III summarizes the absolute magnetic moments per atom for all the considered magnetic 3d metals. We note that, surprisingly, the best results are obtained with the standard DFT method. Although there is no significant difference in magnetic moments computed with the DFT +  $U$ (cLDA) and DFT +  $U$ (cRPA) methods, these values are severely overestimated for Cr and Fe. We note that FM bcc Mn, which is a high-temperature phase of Mn, shows a similar behavior, but experimental reference is missing for this compound. The overestimation of magnetic moments leads to unreasonably large errors in lattice constants of up to 10 % (see Table S3 in the ESI [57]). However, the standard DFT +  $U$  method favors integer orbital occupancies (0 or 1) and localization of electrons, and therefore is known to overestimate magnetic moments [45,74,75]. We note however, that this may be seen also as an artifact of applying the FLL version of DFT +  $U$ , and could be reduced with applying the AMF approach. For the other magnetic elements (Co and Ni), which have higher  $d$  occupation, the differences between the DFT and DFT +  $U$  values are less pronounced, and the agreement with experiment is rather good.

The computed work functions of selected closest-packed crystal surfaces (i.e., (111) for fcc and (110) for bcc struc-

tures) are provided in Table IV. These values were obtained by taking the difference of the surface Fermi energy and the reference electrostatic potential in the middle of the vacuum region. As shown in Table IV, the computed work functions are in most cases smaller than the experimental values. This is consistent with previous calculations using generalized gradient approximation (GGA) and meta-GGA functionals [80,81]. The effect is more pronounced for bcc(110) than for fcc(111) surfaces, with maximal deviations from the experimental values of 0.3 eV. The effect of applying the  $U$  correction is small in most cases. This is expected for  $d$  metals, as the DFT +  $U$  correction simultaneously shifts the energies of the  $d$ -band and the Fermi level, leaving the density of states at the Fermi level unaffected. Except for the case of Pt(111), all computational methods yield very similar values, with larger differences from the measured values than between the methods. The similar values of mean absolute error show that all the methods perform similarly well. Moreover, for the bcc(110) surfaces, the DFT +  $U$ (cLDA) and DFT +  $U$ (cRPA) approaches result in nearly identical work functions values even though the Hubbard  $U$  parameter values differ significantly.

In the next step we computed the  $d$ -bandwidths and  $d$ -band centers for all considered metals. We defined the  $d$ -band center as the centroid of the  $d$ -band and considered two cases: (1) the occupied states (up to the Fermi level) and (2) the entire  $d$ -bandwidth. When computing the  $d$ -bandwidths, we defined the upper and lower limits of the band at points where the  $d$  states DOS is only 5% of the maximum band height. This was done to avoid counting of spurious, minor  $d$  contributions. For spin-polarized metals we considered the sum of spin-up and spin-down components.

As shown in Fig. 3, all methods indicate that 3d metals (except for AFM Cr and FM Mn) have the narrowest bands

TABLE IV. The computed and measured work functions for selected closest-packed metal surfaces (using atomic orbital projectors). The mean absolute deviation (MAD) is reported for each method. The cRPA  $U$  parameters are taken from Ref. [15]. The  $U$  parameter values used in the calculations are given in brackets. All values are in eV.

	Cu(111)	Ag(111)	Pt(111)	Mo(110)	W(110)	MAD
DFT	5.01	4.66	5.82	4.67	4.95	0.15
DFT + $U$ (cLDA)	4.93 (11.7)	4.58 (15.2)	6.19 (3.2)	4.68 (1.8)	5.01 (1.2)	0.17
DFT + $U$ (cRPA)	4.98 (4.9)	4.64 (4.2)	6.19 (3.2)	4.68 (3.1)	5.00 (3.0)	0.15
exp.	4.94 [46], 4.98 [78]	4.74 [78]	5.93 [46,79]	4.95 [78]	5.25 [78]	

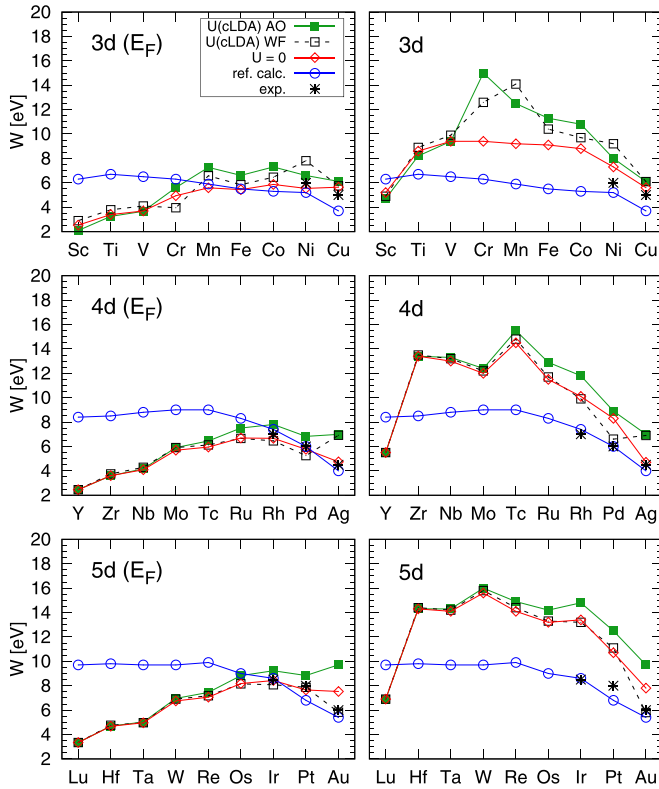


FIG. 3. The  $d$ -bandwidths  $W$  (derived considering: only the occupied part of the  $d$ -band (left panels) and the entire  $d$ -bandwidth (right panels)), derived as described in the text. Magnetic states of Cr, Mn, Fe, Co, and Ni metals are considered. Computed reference data (ref. calc.) are taken from Şaşıoğlu *et al.* [15]. Experimental reference data are taken from Hüfner *et al.* [66] for Ni, Cu and Ag and from Smith *et al.* [82] for Rh, Pd, Ir, Pt, and Au. AO and WF indicate calculations performed with atomic orbitals and Wannier functions as projectors, respectively. Uncertainty of the measured values is in the order of  $\pm 1$  eV, and arises mainly due to unclear definitions of the band limits. All the reported data are also provided in the ESI, Table S4 [57].

compared to their isovalent analogs, while  $5d$  metals have the broadest bands. Along the  $d$  metals series, the bandwidth increases from the start to the middle of the series and slightly decreases for the later transition metals. Data in Fig. 3 indicate also that the DFT +  $U$ (cLDA) method results in broader bands than the standard DFT approach. This effect can also correspond to a shift of the occupied and unoccupied parts of the band to the lower and higher energies, respectively. For all the magnetic  $3d$  metals, the  $U$  correction produces a shift of the spin-up and the spin-down bands relative to each other, broadening the bands.

We note that our computed bandwidths are consistent with the DFT +  $U$  calculations of Cococcioni [47] for Fe bulk, with an increase of  $\sim 2$  eV, when applying the DFT +  $U$  method. The direct comparison to the set of calculated bandwidths of Şaşıoğlu *et al.* [15], as shown in Fig. 3, is not straightforward, since those data were produced applying an unspecified definition of the bandwidth. Figure 3 also shows known measured bandwidths [66,82]. Because XPS measures occupied states, these can be compared to the computed re-

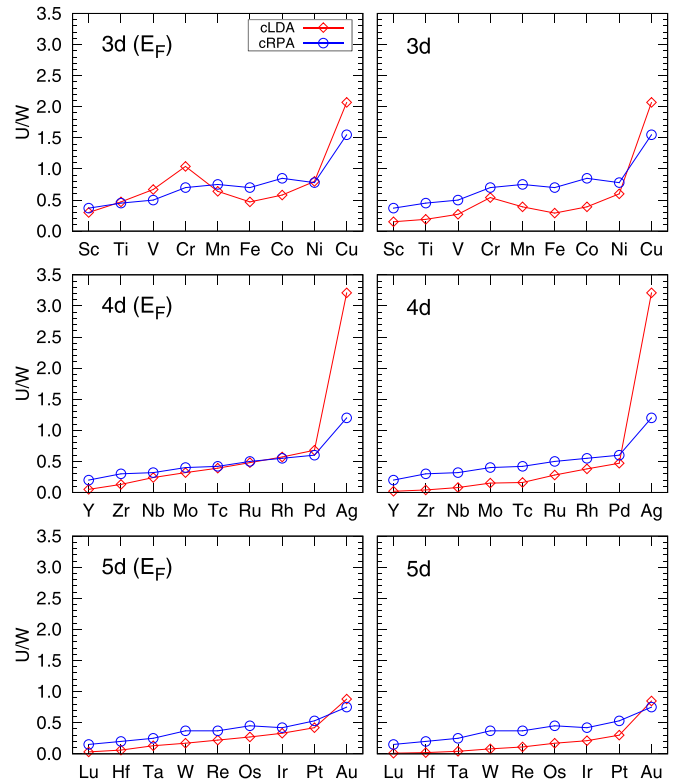


FIG. 4. The  $U/W$  ratio computed with the cLDA and cRPA [15] Hubbard  $U$  parameter values. The bandwidths  $W$  are those from standard DFT calculations ( $U = 0$ ), to allow a straightforward comparison to the cRPA reference data [15] computed in such way. These were derived considering: only the occupied part of the  $d$ -band (left panels) and the entire  $d$ -bandwidth (right panels). Magnetic states of Cr, Mn, Fe, Co, and Ni metals are considered.

sults that account for the occupied part of the  $d$ -band only. We note that the agreement with these experimental data is better in the case of DFT than DFT +  $U$ (cLDA). On the other hand, other spectroscopic studies show that for late transition metals, the  $d$ -bands become narrower with increasing the metal's valence electron number in all periods [82–85]. This trend is also captured in our calculations. We are not aware of similar experimental data for early transition metals, which would be required for more in-depth analysis.

The ratio of computed  $U$  values and the bandwidths,  $U/W$ , is shown in Figure 4. This parameter was used by Şaşıoğlu *et al.* [15] to assess the strength of the electron correlation for the different metals. In agreement with those results, in our calculations the so-defined correlation strength increases along the  $d$  metals series with  $3d$  metals having the largest  $U/W$  ratios. This is because  $3d$  metals have smaller bandwidths and slightly larger  $U$  parameters. The magnetic  $3d$  metals, except for AFM Cr, stand out by relatively small  $U/W$  ratios, thereby significantly differing from the nonmagnetic metal equivalents. We note that due to the large derived  $U$  parameters, Cu and Ag have huge  $U/W$  ratios. This does not necessarily reflect strongly correlated electronic structure, as these elements have completely filled  $d$  shells.

Figure 4 shows that strong correlations ( $U/W > 1$ ) does not occur for the transition metals. Nevertheless, we decided

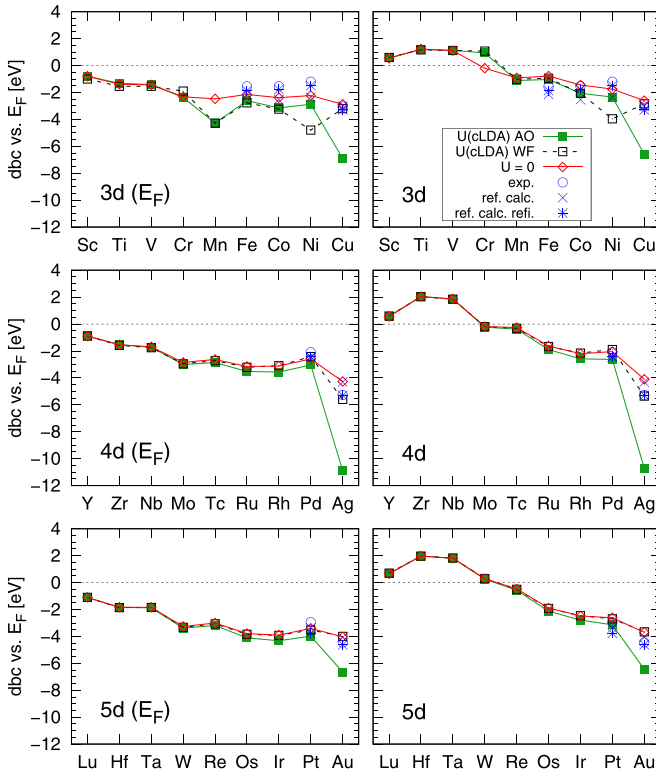


FIG. 5. The position of the  $d$ -band center (dbc) with respect to the Fermi level, derived considering: only the occupied part of the  $d$ -band (left panels) and the entire  $d$ -bandwidth (right panels). Magnetic states of Cr, Mn, Fe, Co, and Ni metals are considered. Experimental XPS data (with maximal uncertainty of  $\pm 0.1$  eV), calculated reference data (standard (ref. calc.) and refined (ref. calc. refi., see the text for explanation)) are taken from Hofmann *et al.* [46] for Fe, Co, Ni, Cu, Pd, Ag, Pt, and Au and from Smith *et al.* [82] for Rh and Ir metals. Refined DFT calculations of Hofmann *et al.* [46] are given by blue stars. More details are provided in the ESI, Table S5 [57].

to test the DFT +  $U$  method for all transition metals, since it is not clear at which point the correlations start to play a significant role [40].

Due to the popularity of the “ $d$ -band model” [35,86], which relates the  $d$ -band center to the adsorption properties on metal surfaces, there exist multiple studies of  $d$ -band centers of different transition metals surfaces [35,80,87]. These show clearly that the  $d$ -band center continuously shifts to lower energies along the  $d$  series, with exceptions only for Ni, Pd, and Pt [80,87]. All studies demonstrate that the 11-valence electrons metals (especially Ag) have very small  $d$ -band center energies. Very similar trends are observed in computational [46] and experimental [46,83,84] studies of the bulk  $d$  metals. The calculated  $d$ -band centers are shown in Fig. 5. The shift to lower energies is reproduced by all the applied methods. Hofmann *et al.* [46] calculated DOS and  $d$ -band centers using the standard DFT method. However, in order to better match the measured spectra, they refined their DOS by varying the  $e_g$  to  $t_{2g}$  orbitals relative contribution ratio and/or applying an offset (represented as “reference refined calculation” in Fig. 5). We note that the difference between bare and refined values is large for Ag.

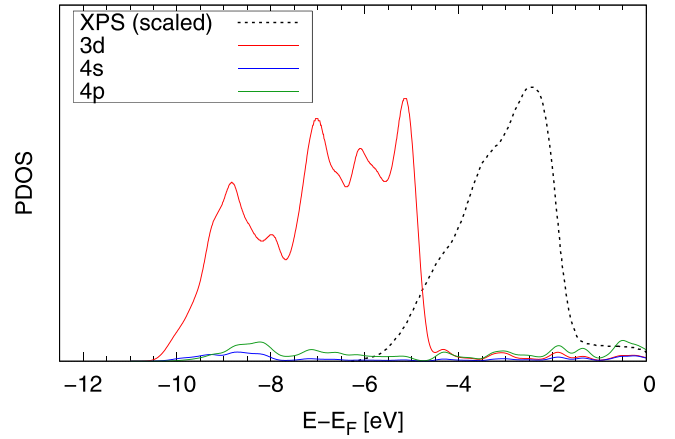


FIG. 6. The projected density of states for fcc Cu computed with the PBEsol +  $U$ (cLDA) method (atomic orbitals as projectors,  $U = 11.7$  eV), with Gaussian smearing of 0.015 Ry. The results show a clear hybrid  $spd$  state between the main  $d$ -band and the Fermi level. XPS data are taken from [46] and scaled vertically to match the intensity of the computed  $d$ -band.

When applying the Hubbard  $U$  correction within the standard FLL scheme, the  $d$ -band centers shift significantly to lower energies, and the shift is proportional to the  $U$  value. The effect reflects a downward energy shift of occupied bands (by  $-0.5U$ ) within the DFT +  $U$  framework. However, the experimental reference is matched much better by the standard DFT results. In particular, as compared to the experimental reference, the DFT +  $U$ (cLDA) results in large shifts of  $d$ -band center energies for Cu, Ag, and Au, in part due to the contribution of  $s$  states to the DOS at the Fermi level (see Fig. 6) [88,89]. The problem of DFT +  $U$  methods in reproducing spectra of transition metals has been noticed before [8,33]. Interestingly, hybrid functionals also have problems in describing metals [90,91], and our simulations of Cu with the hybrid PBE0 functional show the shift and mismatch to the experimental data (see Fig. 2). We will elaborate more on this issue in the next section. We note, however, that the shift of the  $d$ -band is eliminated by the application of the AMF version of the DFT +  $U$  method [8]. Nevertheless, this problem may also be related to the incorrect representation of  $d$  orbitals in metals by atomic  $d$  orbitals used in the projection of  $d$  orbitals occupations, which we discuss in the next section.

#### D. Wannier projectors for $d$ -band properties

Although the DFT +  $U$ (cLDA) method reproduces the periodic trend of  $d$ -band center energies, the absolute energies differ from the measured values by  $\sim 1.5$  eV and by several eV for Cu, Ag, and Au. The experimental bandwidths are also not well matched by the DFT +  $U$ (cLDA) calculations (see Fig. 3). Surprisingly, we note that for metals such as Cu, the standard DFT +  $U$ (cLDA) method results in a shift of the  $d$  levels, but not of the Fermi level itself. To check the reason for such an unexpected behavior we considered the projected DOS. As is shown in Fig. 6, the states at the Fermi level remain unshifted, comparing to the large shift of the  $d$ -band, and they represent a hybrid of  $d$  and  $s$  states. We observe the same behavior for Ag and Au metals. It may in



part originate from the atomic orbital's representation of the  $d$  orbitals that is used in the projection of  $d$  orbitals occupancies in the DFT +  $U$  method. The  $d$  orbitals in metals are different from the equivalent orbitals in isolated atoms, and the usage of an incorrect projector may result in formation of an artificial hybrid orbital at the Fermi level, which could affect the electronic structure computed with the DFT +  $U$  method. On the other hand, it is well known that metals such as Cu possess  $s$ -like contributions at the Fermi level [88,89].

The results of DFT +  $U$  calculations depend on the choice of projector functions [69,92–94]. We address this issue by representing the  $d$  orbitals in metals by Wannier functions. Kvashnina *et al.* [95] have shown that Wannier functions improve the match of the  $f$  electrons DOS to the experimental high resolution x-ray absorption near edge spectra of various uranium oxides. Here we test if similar improvement could be obtained for  $d$  electrons DOS and its match to the measured XPS spectra. The use of Wannier functions is also a common procedure to separate (disentangle) bands [96], and to treat states of mixed character [97]. An overview of the application of Wannier functions in the DFT +  $U$  scheme is given by Himmetoglu *et al.* [43].

We applied maximally localized Wannier functions [52] and obtained a localized basis of orthonormal orbitals to use as projectors of  $d$  orbitals occupancies in the DFT +  $U$  method. We constructed the respective representations of  $d$  states in the Wannier scheme by picking the corresponding band indices. This procedure allowed us to separate  $s$  and  $p$  contributions from the  $d$ -bands. We note, however, that the current implementation of Wannier orbitals does not allow to effectively separate the bands according to their  $s$ ,  $p$  or  $d$  character.

The projected densities of states for the  $d$ -bands calculated with atomic orbitals (AO) and Wannier functions (WF) as projectors are shown for selected elements in Fig. 7, together with the experimental reference. The XPS experimental data of Hofmann *et al.* [46] were measured using Al  $K\alpha$  radiation and include  $s$  and  $p$  contributions, but these are very small [46]. We note that the absolute intensities of computed DOS and XPS data in Fig. 7 are arbitrary and should not be directly compared. This is because of the decrease of relative intensity of XPS bands towards lower energies [46,82] that is attributed to a variation of the photoionization cross section across the  $d$ -band [98]. Moreover, electrons of  $e_g$  symmetry have higher transition probabilities than  $t_{2g}$  electrons [99].

The bands calculated with the DFT +  $U$  method with WF as projectors are much closer in position to the standard DFT and experimental bands (see Figs. 5 and 7). The effect is distinct for Cu, Ag, and Au, with their large  $U$  parameters computed with the cLDA approach. The DFT +  $U$ (cLDA) method with WF is also able to match the experimental  $d$ -band center for Ag, the case for which the standard DFT failed. We note, however, that the WF-based calculations make the prediction for Ni worse. This only happens for the magnetic case, with the nonmagnetic solution showing the same improvement as seen for other metals. This results from general problems in computing the magnetic states with the DFT +  $U$  method (like for the case of Cr, Table III).

The use of WF improves the capability of the DFT +  $U$  scheme for prediction of  $d$ -band centers. Nevertheless, the standard DFT bands still fit the XPS data best. Interestingly,

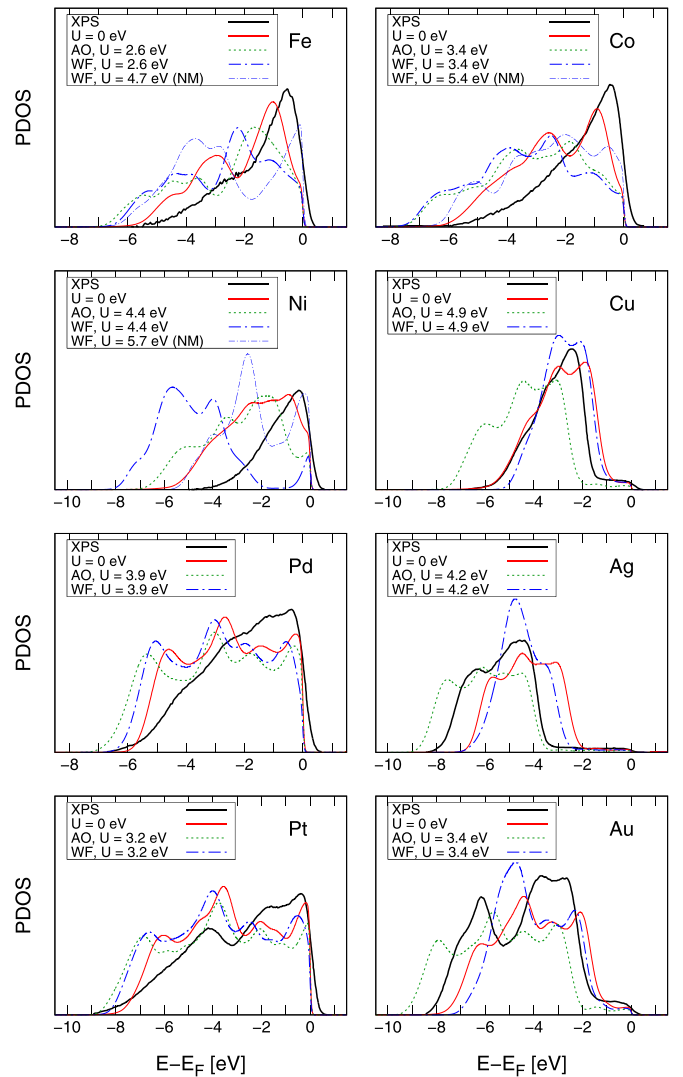


FIG. 7. The projected  $d$  orbitals density of states for selected metals, computed with different projections of  $d$  states occupancy: atomic orbitals (AO), Wannier functions (WF). Gaussian smearing of 0.03 Ry has been applied to match the experimental band broadening. Magnetic and non-magnetic states of Fe, Cr, and Ni metals are considered. XPS data are taken from [46] and are rescaled vertically to match the intensity of the computed  $d$ -bands. The reference experimental spectra agree well with earlier measurements by Höchst *et al.* [101], Hüfner *et al.* [66], Smith *et al.* [82]. Our computed DOS for  $U = 0$  (DFT approach) agree well with the calculations by Hofmann *et al.* [46].

the hybrid functionals also produce a significant, unwanted shift (see Fig. 2). We note, however, that the DFT +  $U$  method corrects only the  $d$  states. Our HF calculations also indicate the need for a correction of the energies of  $s$  states (see estimation of  $U$  parameter values for the lowest occupied valence  $s$  states in Table I). A significant shift of the energies of  $4s$  states we also see in our calculations of Cu (by 2.2 eV) and Gao *et al.* [90] calculations of  $MgB_2$  metals with the PBE0 hybrid functional. Such an unaccounted effect should strongly affect the relative position of  $d$ -band and Fermi level, and potentially improve the match to the XPS spectra [100]. On the other hand, as already discussed, the AMF implementation

of DFT +  $U$  should result in spectral properties similar to the ones obtained with the standard DFT method [8], which gives good results [46]. The spectra of transition metals are also well reproduced with the local spin density approximation plus dynamic mean field theory (LSDA-DMFT) [33].

#### IV. SUMMARY AND CONCLUSIONS

We systematically computed the Hubbard  $U$  parameters for all transition metals using the linear response implementation of the cLDA method, and evaluated the performance of the DFT +  $U$  method for prediction of a set of physical parameters of metal bulk phases and surfaces, elucidating differences between different implementations of the DFT +  $U$  approach. The computed  $U$  parameters compare reasonably well to those obtained with the cRPA method, but show a more pronounced trend along the periodic series. This demonstrates the necessity of using different values of  $U$  parameters for different  $d$  elements. We observe that for metals with fully occupied  $d$  shell (Cu, Ag, Au), the cLDA method overestimates the Hubbard  $U$  parameters, which is a known feature of the method that is attributed to incomplete removal of self-screening. Values consistent with the cLDA and cRPA methods were also obtained with the HF-based estimate proposed here. Such a method results in values and trends along the  $d$  series that surprisingly closely resemble the results of the cRPA method. This indicates that the HF calculations can be used to estimate the values of Hubbard  $U$  parameters.

We also investigated the performance of the DFT +  $U$  method for metallic systems, which are surprisingly well described by the standard DFT approach. In general, the benefit of applying the Hubbard  $U$  correction depends on the element, the property under consideration and the applied DFT +  $U$  scheme. It is important to stress that in the widely used FLL implementation the  $U$  parameter directly affects the position of the  $d$ -band, which is often used as an indicator for adsorption behavior and catalytic activity. We found that the FLL DFT +  $U$  approach overestimates the positions of  $d$ -band centers with respect to the Fermi level, but, interestingly, this is to large extent corrected when the Wannier functions are used as projectors in the determination of occupancies of  $d$  orbitals. We note, however, that such a shift of the  $d$ -band is not expected in the AMF implementation of DFT +  $U$ , which is often referred to as a more appropriate method for computation of metals. The solution of the problem in predicting correct positions of  $d$ -bands may also require simultaneous correction of  $s$  levels that for some metals contribute to the bands at the Fermi level. Nevertheless, our analysis provides a solid basis for the correct computation of electronic structure of metals and metallic surfaces, which is of utmost importance in, for instance, computational catalysis.

#### ACKNOWLEDGMENTS

Computational resources provided by the Jülich Aachen Research Alliance-Center for Simulation and Data Science (JARA-CSD, Project No. cjiek61) are gratefully acknowledged.

- 
- [1] K. Burke, Perspective on density functional theory, *J. Chem. Phys.* **136**, 150901 (2012).
  - [2] A. D. Becke, Perspective: Fifty years of density-functional theory in chemical physics, *J. Chem. Phys.* **140**, 18A301 (2014).
  - [3] S. Jahn and P. M. Kowalski, Theoretical approaches to structure and spectroscopy of earth materials, *Rev. Mineral. Geochem.* **78**, 691 (2014).
  - [4] R. O. Jones, Density functional theory: Its origins, rise to prominence, and future, *Rev. Mod. Phys.* **87**, 897 (2015).
  - [5] A. Jain, Y. Shin, and K. A. Persson, Computational predictions of energy materials using density functional theory, *Nat. Rev. Mater.* **1**, 15004 (2016).
  - [6] N. Mardirossian and M. Head-Gordon, Thirty years of density functional theory in computational chemistry: an overview and extensive assessment of 200 density functionals, *Mol. Phys.* **115**, 2315 (2017).
  - [7] I. G. Austin and N. F. Mott, Metallic and nonmetallic behavior in transition metal oxides, *Science* **168**, 71 (1970).
  - [8] M. Cococcioni and S. de Gironcoli, Linear response approach to the calculation of the effective interaction parameters in the LDA +  $U$  method, *Phys. Rev. B* **71**, 035105 (2005).
  - [9] A. Blanca Romero, P. M. Kowalski, G. Beridze, H. Schlenz, and D. Bosbach, Performance of DFT+ $U$  method for prediction of structural and thermodynamic parameters of monazite-type ceramics, *J. Comput. Chem.* **35**, 1339 (2014).
  - [10] G. Beridze and P. M. Kowalski, Benchmarking the DFT+ $U$  method for thermochemical calculations of uranium molecular compounds and solids, *J. Phys. Chem. A* **118**, 11797 (2014).
  - [11] A. Jain, G. Hautier, S. P. Ong, C. J. Moore, C. C. Fischer, K. A. Persson, and G. Ceder, Formation enthalpies by mixing GGA and GGA+ $U$  calculations, *Phys. Rev. B* **84**, 045115 (2011).
  - [12] V. I. Anisimov, J. Zaanen, and O. K. Andersen, Band theory and Mott insulators: Hubbard  $U$  instead of Stoner  $I$ , *Phys. Rev. B* **44**, 943 (1991).
  - [13] V. I. Anisimov, I. V. Solovyev, M. A. Korotin, M. T. Czyżyk, and G. A. Sawatzky, Density-functional theory and NiO photoemission spectra, *Phys. Rev. B* **48**, 16929 (1993).
  - [14] I. V. Solovyev and P. H. Dederichs, Ab initio calculations of Coulomb  $U$  parameters for transition-metal impurities, *Phys. Rev. B* **49**, 6736 (1994).
  - [15] E. Şaşıoğlu, C. Friedrich, and S. Blügel, Effective Coulomb interaction in transition metals from constrained random-phase approximation, *Phys. Rev. B* **83**, 121101(R) (2011).
  - [16] G.-Y. Huang, C.-Y. Wang, and J.-T. Wang, Detailed check of the LDA+ $U$  and GGA+ $U$  corrected method for defect calculations in wurtzite ZnO, *Comput. Phys. Commun.* **183**, 1749 (2012).
  - [17] S. Laubach, P. C. Schmidt, A. Thißen, F. J. Fernandez-Madrigal, Q.-H. Wu, W. Jaegermann, M. Klemm, and S. Horn, Theoretical and experimental determination of the electronic structure of  $V_2O_5$ , reduced  $V_2O_{5-x}$  and sodium intercalated  $NaV_2O_5$ , *Phys. Chem. Chem. Phys.* **9**, 2564 (2007).

- [18] S. Lutfalla, V. Shapovalov, and A. T. Bell, Calibration of the DFT/GGA+ $u$  method for determination of reduction energies for transition and rare earth metal oxides of Ti, V, Mo, and Ce, *J. Chem. Theory Comput.* **7**, 2218 (2011).
- [19] C. W. M. Castleton, J. Kullgren, and K. Hermansson, Tuning LDA+ $U$  for electron localization and structure at oxygen vacancies in ceria, *J. Chem. Phys.* **127**, 244704 (2007).
- [20] W. Chen, P. Yuan, S. Zhang, Q. Sun, E. Liang, and Y. Jia, Electronic properties of anatase  $\text{TiO}_2$  doped by lanthanides: A DFT+ $U$  study, *Phys. B: Condens. Matter* **407**, 1038 (2012).
- [21] J. T. Pegg, X. Aparicio-Anglès, M. Storr, and N. H. de Leeuw, DFT+ $U$  study of the structures and properties of the actinide dioxides, *J. Nucl. Mater.* **492**, 269 (2017).
- [22] C. Herring, in *Magnetism*, edited by G. T. Rado, and H. Suhl (Academic Press, New York, 1966), pp. 187–240.
- [23] B. N. Cox, M. A. Coulthard, and P. Lloyd, A calculation of the Coulomb correlation energy,  $U$ , for transition metals in Hubbard's model, *J. Phys. F* **4**, 807 (1974).
- [24] V. I. Anisimov and O. Gunnarsson, Density-functional calculation of effective Coulomb interactions in metals, *Phys. Rev. B* **43**, 7570 (1991).
- [25] I. Schnell, G. Czycholl, and R. C. Albers, Hubbard- $U$  calculations for Cu from first-principle Wannier functions, *Phys. Rev. B* **65**, 075103 (2002).
- [26] K. Nakamura, R. Arita, Y. Yoshimoto, and S. Tsuneyuki, First-principles calculation of effective onsite Coulomb interactions of  $3d$  transition metals: Constrained local density functional approach with maximally localized Wannier functions, *Phys. Rev. B* **74**, 235113 (2006).
- [27] N. J. Mosey and E. A. Carter, *Ab initio* evaluation of Coulomb and exchange parameters for DFT+  $U$  calculations, *Phys. Rev. B* **76**, 155123 (2007).
- [28] N. J. Mosey, P. Liao, and E. A. Carter, Rotationally invariant *ab initio* evaluation of Coulomb and exchange parameters for DFT+  $U$  calculations, *J. Chem. Phys.* **129**, 014103 (2008).
- [29] M. Springer and F. Aryasetiawan, Frequency-dependent screened interaction in Ni within the random-phase approximation, *Phys. Rev. B* **57**, 4364 (1998).
- [30] F. Aryasetiawan, M. Imada, A. Georges, G. Kotliar, S. Biermann, and A. I. Lichtenstein, Frequency-dependent local interactions and low-energy effective models from electronic structure calculations, *Phys. Rev. B* **70**, 195104 (2004).
- [31] F. Aryasetiawan, K. Karlsson, O. Jepsen, and U. Schönberger, Calculations of Hubbard  $U$  from first-principles, *Phys. Rev. B* **74**, 125106 (2006).
- [32] I. V. Solov'yev and M. Imada, Screening of coulomb interactions in transition metals, *Phys. Rev. B* **71**, 045103 (2005).
- [33] J. Minár, Correlation effects in transition metals and their alloys studied using the fully self-consistent KKR-based LSDA DMFT scheme, *J. Phys.: Condens. Matter* **23**, 253201 (2011).
- [34] G. Lan, J. Song, and Z. Yang, A linear response approach to determine Hubbard  $u$  and its application to evaluate properties of  $\text{Y}_2\text{B}_2\text{O}_7$ ,  $b = \text{transition metals } 3d, 4d \text{ and } 5d$ , *J. Alloys Compd.* **749**, 909 (2018).
- [35] A. Ruban, B. Hammer, P. Stoltze, H. Skriver, and J. Nørskov, Surface electronic structure and reactivity of transition and noble metals, *J. Mol. Catal. A Chem.* **115**, 421 (1997).
- [36] B. Hammer, L. B. Hansen, and J. K. Nørskov, Improved adsorption energetics within density-functional theory using revised Perdew-Burke-Ernzerhof functionals, *Phys. Rev. B* **59**, 7413 (1999).
- [37] M. Gajdoš and J. Hafner, Co adsorption on Cu(111) and Cu(001) surfaces: Improving site preference in DFT calculations, *Surf. Sci.* **590**, 117 (2005).
- [38] S. Gautier, S. N. Steinmann, C. Michel, P. Fleurat-Lessard, and P. Sautet, Molecular adsorption at Pt(111). How accurate are DFT functionals? *Phys. Chem. Chem. Phys.* **17**, 28921 (2015).
- [39] G. Kotliar, S. Y. Savrasov, K. Haule, V. S. Oudovenko, O. Parcollet, and C. A. Marianetti, Electronic structure calculations with dynamical mean-field theory, *Rev. Mod. Phys.* **78**, 865 (2006).
- [40] A. G. Petukhov, I. I. Mazin, L. Chioncel, and A. I. Lichtenstein, Correlated metals and the LDA +  $U$  method, *Phys. Rev. B* **67**, 153106 (2003).
- [41] M. T. Czyżyk and G. A. Sawatzky, Local-density functional and on-site correlations: The electronic structure of  $\text{La}_2\text{CuO}_4$  and  $\text{LaCuO}_3$ , *Phys. Rev. B* **49**, 14211 (1994).
- [42] S. Ryee and M. J. Han, The effect of double counting, spin density, and hund interaction in the different DFT+ $U$  functionals, *Sci. Rep.* **8**, 9559 (2018).
- [43] B. Himmetoglu, A. Floris, S. de Gironcoli, and M. Cococcioni, Hubbard-corrected DFT energy functionals: The LDA+ $U$  description of correlated systems, *Int. J. Quantum Chem.* **114**, 14 (2014).
- [44] I. Yang, S. Y. Savrasov, and G. Kotliar, Importance of Correlation Effects on Magnetic Anisotropy in Fe and Ni, *Phys. Rev. Lett.* **87**, 216405 (2001).
- [45] Y. Shoaib Mohammed, Y. Yan, H. Wang, K. Li, and X. Du, Stability of ferromagnetism in fe, co, and ni metals under high pressure with GGA and GGA+ $U$ , *J. Magn. Magn. Mater.* **322**, 653 (2010).
- [46] T. Hofmann, T. H. Yu, M. Folse, L. Weinhardt, M. Bär, Y. Zhang, B. V. Merinov, D. J. Myers, W. A. Goddard III, and C. Heske, Using photoelectron spectroscopy and quantum mechanics to determine  $d$ -band energies of metals for catalytic applications, *J. Phys. Chem. C* **116**, 24016 (2012).
- [47] M. Cococcioni, A LDA+ $U$  study of selected iron compounds, Ph.D. thesis, International School for Advanced Studies-SISSA, Trieste, 2002.
- [48] P. Giannozzi, S. Baroni, N. Bonini, M. Calandra, R. Car, C. Cavazzoni, D. Ceresoli, G. L. Chiarotti, M. Cococcioni, I. Dabo, A. D. Corso, S. de Gironcoli, S. Fabris, G. Fratesi, R. Gebauer, U. Gerstmann, C. Gougoussis, A. Kokalj, M. Lazzeri, L. Martin-Samos *et al.*, QUANTUM ESPRESSO: A modular and open-source software project for quantum simulations of materials, *J. Phys.: Condens. Matter* **21**, 395502 (2009).
- [49] J. P. Perdew, A. Ruzsinszky, G. I. Csonka, O. A. Vydrov, G. E. Scuseria, L. A. Constantin, X. Zhou, and K. Burke, Restoring the Density-Gradient Expansion for Exchange in Solids and Surfaces, *Phys. Rev. Lett.* **100**, 136406 (2008).
- [50] J. P. Perdew, K. Burke, and M. Ernzerhof, Generalized Gradient Approximation Made Simple, *Phys. Rev. Lett.* **77**, 3865 (1996).
- [51] H. J. Monkhorst and J. D. Pack, Special points for Brillouin-zone integrations, *Phys. Rev. B* **13**, 5188 (1976).
- [52] N. Marzari and D. Vanderbilt, Maximally localized generalized Wannier functions for composite energy bands, *Phys. Rev. B* **56**, 12847 (1997).

- [53] D. K. G. de Boer, C. Haas, and G. A. Sawatzky, Auger spectra of compounds of Sc, Ti and Cr, *J. Phys. F* **14**, 2769 (1984).
- [54] G. A. Sawatzky and D. Post, X-ray photoelectron and Auger spectroscopy study of some vanadium oxides, *Phys. Rev. B* **20**, 1546 (1979).
- [55] E. Antonides, E. C. Janse, and G. A. Sawatzky, LMM Auger spectra of Cu, Zn, Ga, and Ge. I. Transition probabilities, term splittings, and effective Coulomb interaction, *Phys. Rev. B* **15**, 1669 (1977).
- [56] T. Kaurila, J. Väyrynen, and M. Isokallio, Experimental study of resonant photoemission in the metals V, Cr, Mn, and Co, *J. Phys.: Condens. Matter* **9**, 6533 (1997).
- [57] See Supplemental Material at <http://link.aps.org/supplemental/10.1103/PhysRevB.105.195153> for tabulated data from the figures, structures of the elements and all computed and experimental lattice parameters.
- [58] J. W. Bennett, B. G. Hudson, I. K. Metz, D. Liang, S. Spurgeon, Q. Cui, and S. E. Mason, A systematic determination of Hubbard U using the GBRV ultrasoft pseudopotential set, *Comput. Mater. Sci.* **170**, 109137 (2019).
- [59] T. Koopmans, Über die Zuordnung von Wellenfunktionen und Eigenwerten zu den einzelnen Elektronen eines Atoms, *Physica* **1**, 104 (1934).
- [60] F. J. Galvez, E. Buendia, P. Maldonado, and A. J. Sarsa, Optimized effective potential energies and ionization potentials for the atoms Li to Ra *Eur. Phys. J. D* **50**, 229 (2008).
- [61] S. L. Dudarev, G. A. Botton, S. Y. Savrasov, C. J. Humphreys, and A. P. Sutton, Electron-energy-loss spectra and the structural stability of nickel oxide: An LSDA+U study, *Phys. Rev. B* **57**, 1505 (1998).
- [62] C. Adamo and V. Barone, Toward reliable density functional methods without adjustable parameters: The PBE0 model, *J. Chem. Phys.* **110**, 6158 (1999).
- [63] G. Shamov, G. Schreckenbach, and T. Vo, A comparative relativistic DFT and *ab initio* study on the structure and thermodynamics of the oxofluorides of uranium(IV), (V), and (VI), *Chem. Eur. J.* **13**, 4932 (2007).
- [64] J. P. Perdew, M. Ernzerhof, and K. Burke, Rationale for mixing exact exchange with density functional approximations, *J. Chem. Phys.* **105**, 9982 (1996).
- [65] C. N. Berglund and W. E. Spicer, Photoemission studies of copper and silver: Experiment, *Phys. Rev.* **136**, A1044 (1964).
- [66] S. Hüfner, G. Wertheim, N. Smith, and M. Traum, XPS density of states of copper, silver, and nickel, *Solid State Commun.* **11**, 323 (1972).
- [67] I. Schnell, G. Czycholl, and R. C. Albers, Unscreened Hartree-Fock calculations for metallic Fe, Co, Ni, and Cu from *ab initio* Hamiltonians, *Phys. Rev. B* **68**, 245102 (2003).
- [68] C. S. Lawson, B. J. Tielsch, and J. E. Fulghum, Study of the first row transition metals by X-ray photoelectron spectroscopy, *Surf. Sci. Spectra* **4**, 316 (1996).
- [69] Á. Morales-García, S. Rhatigan, M. Nolan, and F. Illas, On the use of DFT+U to describe the electronic structure of TiO<sub>2</sub> nanoparticles: (TiO<sub>2</sub>)<sub>35</sub> as a case study, *J. Chem. Phys.* **152**, 244107 (2020).
- [70] W. E. Pickett, S. C. Erwin, and E. C. Ethridge, Reformulation of the LDA + U method for a local-orbital basis, *Phys. Rev. B* **58**, 1201 (1998).
- [71] G. Bergerhoff and I. D. Brown, ICSD database, in *Crystallographic Databases*, edited by F. Allen (International Union of Crystallography, Chester, 1987).
- [72] D. R. Lide (ed.), Properties of solids; Thermal and physical properties of pure metals, in *CRC Handbook of Chemistry and Physics* (CRC Press, Boca Raton, Florida, 2003), 84th ed., pp. 12–219.
- [73] G.-X. Zhang, A. M. Reilly, A. Tkatchenko, and M. Scheffler, Performance of various density-functional approximations for cohesive properties of 64 bulk solids, *New J. Phys.* **20**, 063020 (2018).
- [74] E. R. Ylvisaker, W. E. Pickett, and K. Koepnick, Anisotropy and magnetism in the LSDA + U method, *Phys. Rev. B* **79**, 035103 (2009).
- [75] Y. Fu and D. J. Singh, Density functional methods for the magnetism of transition metals: SCAN in relation to other functionals, *Phys. Rev. B* **100**, 045126 (2019).
- [76] J. Kübler, Spin-density functional calculations for chromium, *J. Magn. Magn. Mater.* **20**, 277 (1980).
- [77] J. Trygg, B. Johansson, O. Eriksson, and J. M. Wills, Total Energy Calculation of the Magnetocrystalline Anisotropy Energy in the Ferromagnetic 3d Metals, *Phys. Rev. Lett.* **75**, 2871 (1995).
- [78] H. B. Michaelson, The work function of the elements and its periodicity, *J. Appl. Phys.* **48**, 4729 (1977).
- [79] B. Nieuwenhuys and W. Sachtler, Crystal face specificity of nitrogen adsorption on a platinum field emission tip, *Surf. Sci.* **34**, 317 (1973).
- [80] M. Gajdoš, A. Eichler, and J. Hafner, CO adsorption on close-packed transition and noble metal surfaces: Trends from *ab initio* calculations, *J. Phys.: Condens. Matter* **16**, 1141 (2004).
- [81] A. Patra, J. E. Bates, J. Sun, and J. P. Perdew, Properties of real metallic surfaces: Effects of density functional semilocality and van der Waals nonlocality, *Proc. Natl. Acad. Sci.* **114**, E9188 (2017).
- [82] N. V. Smith, G. K. Wertheim, S. Hüfner, and M. M. Traum, Photoemission spectra and band structures of d-band metals. IV. X-ray photoemission spectra and densities of states in Rh, Pd, Ag, Ir, Pt, and Au, *Phys. Rev. B* **10**, 3197 (1974).
- [83] L. H. Bennett, ed., *Electronic Density of States*, Institute for Materials Research (National Bureau of Standards, Washington, 1971).
- [84] S. Hüfner and G. Wertheim, X-ray photoemission studies of the 3d metals from Mn to Cu, *Phys. Lett. A* **47**, 349 (1974).
- [85] W. Speier, J. C. Fuggle, R. Zeller, B. Ackermann, K. Szot, F. U. Hillebrecht, and M. Campagna, Bremsstrahlung isochromat spectra and density-of-states calculations for the 3d and 4d transition metals, *Phys. Rev. B* **30**, 6921 (1984).
- [86] B. Hammer and J. K. Nørskov, Why gold is the noblest of all the metals, *Nature (London)* **376**, 238 (1995).
- [87] A. Vojvodic, J. K. Nørskov, and F. Abild-Pedersen, Electronic structure effects in transition metal surface chemistry, *Top. Catal.* **57**, 25 (2014).
- [88] G. A. Burdick, Energy band structure of copper, *Phys. Rev.* **129**, 138 (1963).



- [89] O. Jepsen, D. Glötzel, and A. R. Mackintosh, Potentials, band structures, and Fermi surfaces in the noble metals, *Phys. Rev. B* **23**, 2684 (1981).
- [90] W. Gao, T. A. Abtew, T. Cai, Y.-Y. Sun, S. Zhang, and P. Zhang, On the applicability of hybrid functionals for predicting fundamental properties of metals, *Solid State Commun.* **234-235**, 10 (2016).
- [91] J. Paier, M. Marsman, and G. Kresse, Why does the B3LYP hybrid functional fail for metals? *J. Chem. Phys.* **127**, 024103 (2007).
- [92] M. Kick, K. Reuter, and H. Oberhofer, Intricacies of DFT+ $U$ , not only in a numeric atom centered orbital framework, *J. Chem. Theory Comput.* **15**, 1705 (2019).
- [93] P. M. Kowalski, Z. He, and O. Cheong, Electrode and electrolyte materials from atomistic simulations: Properties of  $\text{Li}_x\text{FePO}_4$  electrode and zircon-based ionic conductors, *Front. Energy Res.* **9**, 653542 (2021).
- [94] G. L. Murphy, Z. Zhang, R. Tesch, P. M. Kowalski, M. Avdeev, E. Y. Kuo, D. J. Gregg, P. Kegler, E. V. Alekseev, and B. J. Kennedy, Tilting and distortion in rutile-related mixed metal ternary uranium oxides: A structural, spectroscopic, and theoretical investigation, *Inorg. Chem.* **60**, 2246 (2021).
- [95] K. O. Kvashnina, P. M. Kowalski, S. M. Butorin, G. Leinders, J. Pakarinen, R. Bès, H. Li, and M. Verwerft, Trends in the valence band electronic structures of mixed uranium oxides, *Chem. Commun.* **54**, 9757 (2018).
- [96] I. Souza, N. Marzari, and D. Vanderbilt, Maximally localized Wannier functions for entangled energy bands, *Phys. Rev. B* **65**, 035109 (2001).
- [97] D. Novoselov, D. M. Korotin, and V. I. Anisimov, Hellmann-Feynman forces within the DFT +  $U$  in Wannier functions basis, *J. Phys.: Condens. Matter* **27**, 325602 (2015).
- [98] N. J. Shevchik, X-ray photoionization cross sections of  $d$ -band metals, *Phys. Rev. B* **13**, 4217 (1976).
- [99] V. Nemoskalenko, V. Aleshin, Y. Kucherenko, and L. Sheludchenko, Transition probability effect on the shape of electron energy distribution in x-ray electron spectra of copper, silver and palladium, *J. Electron Spectrosc. Relat. Phenom.* **6**, 145 (1975).
- [100] Unfortunately, it is not possible to apply a  $U$  correction to more than one orbital ( $l$  quantum number) of the same element in the current release of Quantum ESPRESSO package (version 6.5).
- [101] H. Höchst, S. Hüfner, and A. Goldmann, XPS-valence bands of iron, cobalt, palladium, and platinum, *Phys. Lett. A* **57**, 265 (1976).